Improved Isotopic Analysis With a Large Array of Gamma-Ray Microcalorimeters

N. Jethava, J. N. Ullom, D. A. Bennett, W. B. Doriese, J. A. Beall, G. C. Hilton, R. D. Horansky, K. D. Irwin, E. Sassi, L. R. Vale, M. K. Bacrania, A. S. Hoover, P. J. Karpius, M. W. Rabin, C. R. Rudy, and D. T. Vo

Abstract—We present results from the largest array of gamma-ray microcalorimeters operated to date. The microcalorimeters consist of Mo/Cu transition-edge sensors with attached Sn absorbers. The detector array contains 66 pixels each with an active area 2.25 mm^2. Out of 66 pixels, 55 are active, and 31 were used to acquire a high statistics Pu gamma-ray spectrum. The energy resolution of the best 21 pixels was found to be 120 eV FWHM. The array is read out using time domain SQUID multiplexing. Here, we describe the multiplexing and present a high statistics Pu spectra. Because of the large collecting area of our array, the statistical error in the ^{240}Pu line intensity is approximately 0.7%, which is comparable to the systematic error in a measurement with a 500 eV germanium sensor. Hence, we have reached an important threshold for demonstrating improved isotopic measurements with microcalorimeter sensors. With straightforward changes, we plan to achieve a resolution of about 50 eV FWHM with 256 multiplexed detectors. Finally, we present early estimates of on-chip heating within our sensor array.

Index Terms—Gamma-ray microcalorimeter, plutonium isotopics, SQUID multiplexing, transition edge sensor.

I. INTRODUCTION

TRANSITION edge sensors (TESs) are increasingly used in microcalorimeters and microbolometers for applications ranging from materials analysis to astronomical imaging. In a microcalorimeter, the energy of an incident photon is determined by measuring the temperature rise it causes in the device. A microcalorimeter consists of three parts: an absorber, a sensitive thermistor that measures the temperature rise, and a weak thermal link to the bath. TES microcalorimeters are generally operated at subkelvin temperatures and, as a result, their spectral resolution is ~10 times better than the germanium detectors that are typically used for high-resolution gamma-ray spectroscopy [1], [2]. However, the area of a high-quality germanium detector can be several hundred mm^2, whereas the typical area of a microcalorimeter is of order 1 mm^2.

As a result, for gamma-ray microcalorimeters to be useful in practical measurement scenarios, multiplexed arrays are required. Detector arrays provide increased collection area and count rate, while multiplexing (combining the signal from multiple sensors into a single amplifier chain) reduces the number of readout amplifiers and the complexity of the associated wiring. NIST is actively involved in developing large-format TES arrays read out using time-domain multiplexing (TDM) techniques [3]–[6]. An alternative readout scheme is frequency-domain multiplexing [7].

Here, we demonstrate the use of TDM with an array of gamma-ray microcalorimeters. In TES readout applications, each TES is operated in parallel with a load resistance R_L and connected in series with the input coil of a first stage SQUID current amplifier. In TDM, the first stage SQUIDs are turned on one at a time, and their outputs are measured by shared second and third stage SQUIDs. Presently, the SQUID switching occurs on timescales of about 1 μs. For these relatively long times, experimental techniques familiar in cryogenic detector work can be used, including low-power twisted-pair wiring and low-noise SQUID amplifiers with a few megahertz of bandwidth [4].

The NIST TDM scheme is designed for two-dimensional (2D) arrays. For 2D multiplexing, the signals from each column of detectors are present on the output of a shared SQUID series array, which is the third stage of SQUID amplification. Digital electronics provide address currents, I_{ad}, to each row of first stage SQUIDs. Digital electronics also supply a feedback current, I_{fb}, to the active first stage SQUID of each column. After waiting for a settling time, t_{set}, the error signal is averaged, and a new feedback signal is computed for when the row is next addressed. Once the addressing of a row is finished, I_{ad} and V_{fb} are turned off, and same sequence is repeated for the next row.

We present early results from the largest gamma-ray microcalorimeter array demonstrated to date. A large collecting area is desirable for nuclear materials analysis, e.g. determination of plutonium isotopes in complex mixtures and determination of the plutonium content in spent reactor fuel [8].

II. EXPERIMENTAL SETUP

The TESs used in this experiment are optimized for observing gamma-rays in the 100 keV to 130 keV region. The thermistors are Mo/Cu bilayers with transition temperatures near 140 mK and normal resistances of about 8 mΩ. The Mo is 0.1 μm thick and the Cu is 0.2 μm thick. Each pixel has a $1.5 \times 1.5 \times 0.25$ mm^3 Sn absorber. Fig. 1 shows the detector chip, called a "Texas chip", containing 66 pixels. We achieved 100% yield on
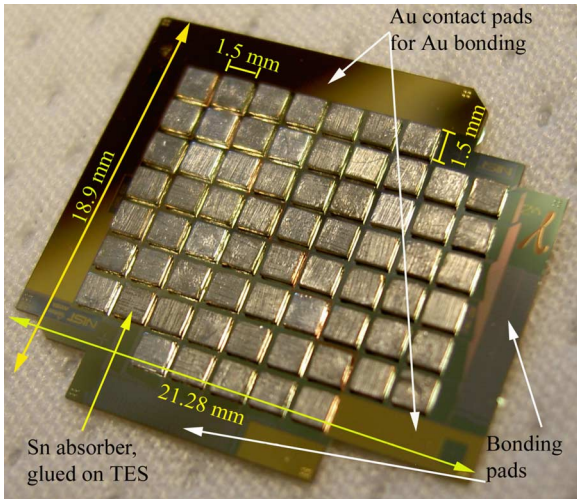
Fig. 1. Si chip containing 66 detectors, out of which 31 were used to acquire a high statistics Pu spectrum. A detector pixel consists of a superconducting Sn absorber ($1.5 \, \text{mm} \times 1.5 \, \text{mm} \times 250 \, \mu\text{m}$) glued to a Mo/Cu TES bilayer. Absorber attachment yield was 100%. An Au film $0.1 \, \mu\text{m}$ thick is deposited along the edges of the array. During experiments, two of the array edges are wire bonded to the assembly box using Au wires. The Si chip is $250 \, \mu\text{m}$ thick. A $0.5 \, \mu\text{m}$ thick Au mesh is deposited at the back-side of the array to improve the thermalization of the chip. Since each multiplexer chip can address only 32 detectors, two of the 66 pixels on the detector chip are considered spares.
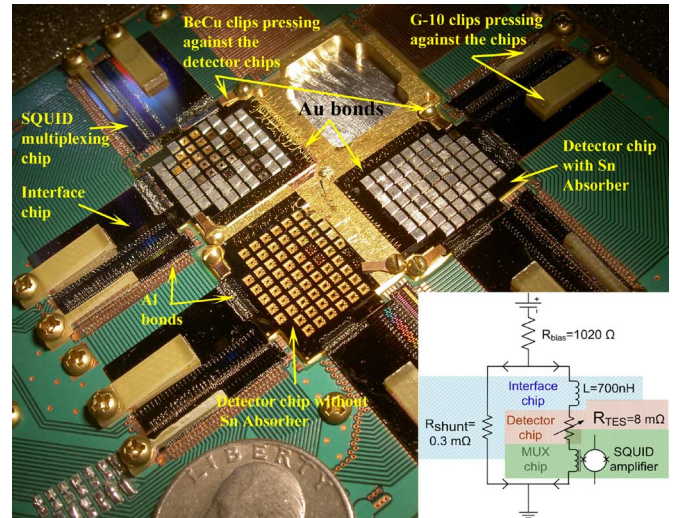

Fig. 2. Photograph of detector chips mounted inside the sample box. The box contains an array with all 66 absorbers, an array without any absorbers, and an earlier array where the absorber attachment was only partially successful. It is possible to mount four detector arrays with 64 live pixels each, making it possible observe with 256 detectors. The inset shows the bias circuit for a single sensor. An extra inductor of 700 nH is placed in the TES circuit to bandwidth limit the readout circuit and increase the rise time of each pulse. The detailed electrical wiring diagram for NIST SQUID chips is explained in the literature [9], [10].

Sn absorber attachment. The Sn absorber is attached with Stycast-1266 to eight posts made from a photopatternable epoxy. These eight posts are connected to the thermistor by a thin film of Cu. The individual pixels have increased dynamic range and better linearity than our previous designs to facilitate high precision measurements of Pu isotopes.

In order to thermalize the detector chip, an Au film is deposited along the edges of the front side. In addition, an Au film is deposited on the entire back of the array except for the sensor membranes. Au bonding wires connect some regions of the front-side gold to the bulk metal of the cryostat.

As shown in Fig. 2, detector chips are installed inside a gold plated copper box. The box can accommodate up to four chips. A printed circuit board (PCB) is also mounted in the box. The board is divided into eight bays (or columns), each with a SQUID multiplexer chip containing 32 first stage SQUID switches and a shared second stage SQUID. Each bay also contains an interface chip. The interface chip provides the shunt resistor and an extra series inductance for each TES. The 32 row addresses on each MUX chip are connected in series for the eight bays. Hence, each of the 32 rows addresses circles clockwise on the PCB shown in Fig. 2. Eight third stage SQUID series array amplifiers are mounted on the 4 K stage of the cryostat (not shown). All signals are carried from the detector box to the 4 K stage on commercial cables made of twisted pairs of CuNi-NbTi wire. These cables have an intermediate heat sink at approximately 1 K. All signals are carried from the 4 K stage to 300 K on striplines of CuNi on kapton. The detector box is placed inside single layers of cryoperm and niobium shielding which are attached to the 4 K stage.

Multiplexing parameters such as the settling time and the number of pixels per column must be optimized so that there is no degradation of detector performance. These parameters were obtained while initially multiplexing only two detectors. In our digital electronics, a sampling period of 80 ns is required to measure the output of each row. However, for the present cryostat wiring, there is a $1.52 \, \mu\text{s}$ switching transient after turning on each row address. To avoid performance degradation, the detector output can be sampled only after waiting for the settling period. Thus, each detector pixel is sampled every $N \times 1.6 \, \mu\text{s}$, where N is the number of pixels in the column. As a result of this finite sampling, there is a significant error signal during the initial rapid rise of a gamma-ray pulse. For $N = 2$, the error signal is approximately 30 mV, compared to the full 240 mV amplitude of the three stage SQUID $V - \Phi$ curve. Crudely, the error signal grows linearly with the number of detectors. As a result, it is possible to multiplex $240 \, \text{mV}/30 \, \text{mV} = 8 \times 2 = 16 \, \text{detectors}$ in a single column. In practice, 14 rows were multiplexed in each column. We foresee two routes to improve the performance of the multiplexing system. We have previously achieved settling periods of about 700 ns in another experimental setup at NIST [11]. Shortening the settling period by this amount will roughly halve the error flux. In addition, the inductance in the TES bias circuit (shown in Fig. 2) can be further increased, thus slowing the rise of the pulses. Combining these improvements, we expect to multiplex 32 rows per column. The sample box of Fig. 2 is maintained at a temperature of 80 mK during experiments by a two-stage adiabatic demagnetization refrigerator (ADR). The ADR is attached to a two-stage pulse tube cooler, which is operated at ∼4 K. Hence, no liquid cryogens are required.

III. EXPERIMENTAL RESULTS

We performed a 20.2 hour measurement of a mixed isotope Pu sample (New Brunswick Laboratory CRM-138, 8% ^{240}Pu). The data set contained 37.98 million pulses. Reduced data in
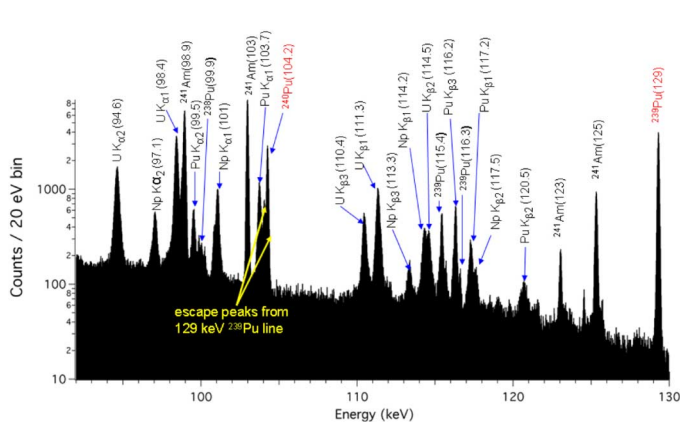
Fig. 3. Pu spectra showing numerous X-rays and gamma-rays. The ^{239}Pu and ^{240}Pu gamma-rays at 129.3 and 104.2 keV, respectively, are used for isotopic analysis. The spectrum is from the best 21 pixels whose average energy resolution is 120 eV. For comparison, the energy resolution of competing germanium sensors is 400–500 eV, which obscures the ^{240}Pu line at 104.2 keV.

the energy range 92 to 130 keV is shown in Fig. 3. Pulses were checked for pile-up, optimally filtered, energy calibrated, and drift corrected. A large number of gamma- and X-rays are visible in Fig. 3. In particular, intense gamma-rays from ^{239}Pu (^{240}Pu) are visible at 129.3 (104.2) keV. These are the preferred gamma-rays for determining the ^{240}Pu/^{239}Pu ratio. This ratio is an important indicator of the purpose and manufacturing history of a Pu sample. If the ratio is above 0.075, then material is considered as 'reactor grade', while if the ratio is below 0.075, it is considered 'weapons grade' [12].

For germanium sensors with resolution 400 eV–500 eV FWHM, the ^{240}Pu line at 104.2 keV is partially obscured by the Pu X-ray at 103.7 keV. This overlap produces a systematic error of order 1% in the ^{240}Pu determination [13]. As shown in Fig. 3, the improved resolution of the microcalorimeter eliminates this overlap and, hopefully, the associated systematic error. A requirement for a useful microcalorimeter measurement is that the statistical error from the number of counts be smaller than the systematic error in a competing germanium measurement. A microcalorimeter measurement must contain greater than 10^4 counts in the 104.2 keV 240Pu line to meet this criteria. The spectrum in Fig. 3 contains more than 1.8×10^4 counts in the 104.2 keV line indicating that, for the first time, a microcalorimeter Pu measurement has crossed the statistical threshold for practical use. More detailed analysis of the spectrum in Fig. 3 is ongoing. One complication is the presence of Sn escape lines at 104 and 104.3 keV.

The strong 60 keV ^{241}Am line (not shown in Fig. 3) is approximately 20 times brighter than the Pu lines near 100 keV. The 60 keV line is an additional complication during Pu measurements since these photons increase the dead time of the detectors. As result, we performed several initial data acquisition runs with different thicknesses of Cadmium (Cd) sheet placed between the radioactive source and cryostat to act as a low energy attenuator. Our measurements showed that 1 mm of Cd increased the ratio of 100 keV/60 keV photons by a factor of 3.6. Consequently, 1 mm of Cd was used during the high statistics pulses acquisition.
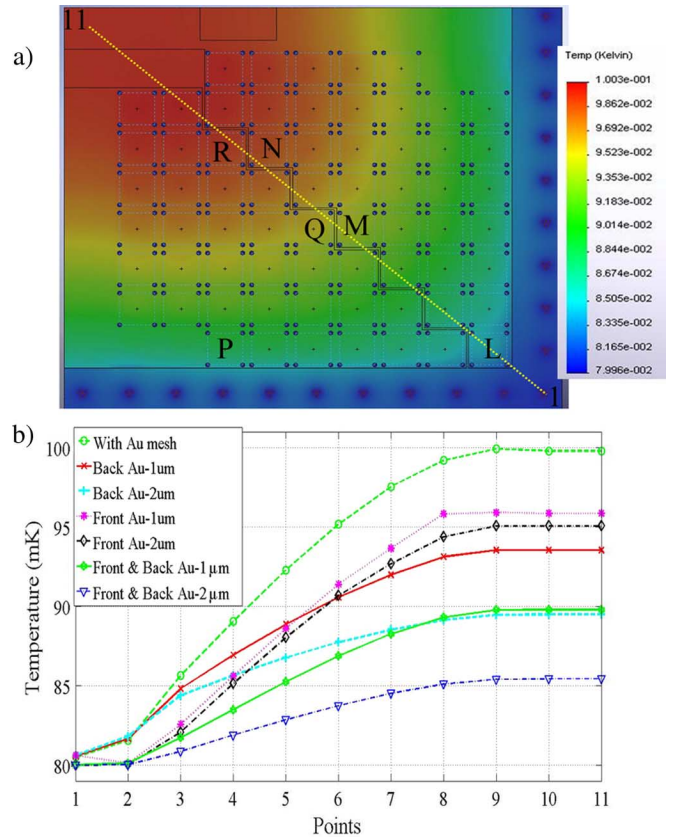

Fig. 4. (a) Predictions of finite element analysis of the detector chip. The base temperature was fixed at 80 mK and each detector dissipates 100 pW of bias power. Au wire bonds connect Au films on the right and bottom edges of the chip to the bulk metal of the cryostat. No heat is allowed to exit the back side of the chip. (b) Predicted temperature distribution in the array along the line indicated by points 1 and 11. The dashed curve with circular markers (green) corresponds to the experimental situation. Simulations of other geometries with thicker Au on the front and back of the chip are also indicated.

In another series of test acquisitions, we determined that the input count rate strongly affects the resolution of the detectors, presumably due to a combination of crosstalk and unremoved pile up. During the high statistics data, the input count rate was 20 Hz, which resulted in the 120 eV resolution shown in Fig. 3. At a 10 Hz input count rate, the energy resolution was estimated to be about 70 eV.

During gamma-ray measurements, the detectors were maintained at approximately 25% of their normal state resistance. This bias point was the steepest part of the transition and provided the shortest time constant and best signal-to-noise ratio.

IV. CHIP HEATING

Since each of the 64 active pixels on the chip dissipates ∼100 pW when biased, it is natural to suspect that the temperature of the detector chip exceeds that of the cryostat. The detectors are biased in two columns of 32. We observed that biasing one column affects the current-voltage characteristics of the other column. Hence, there is steady-state heating of the chip. During spectral measurements, the detectors absorb photons. Since the heat sinking of the chip is not perfect, it is also likely that absorption events introduce thermal cross talk between pixels. In
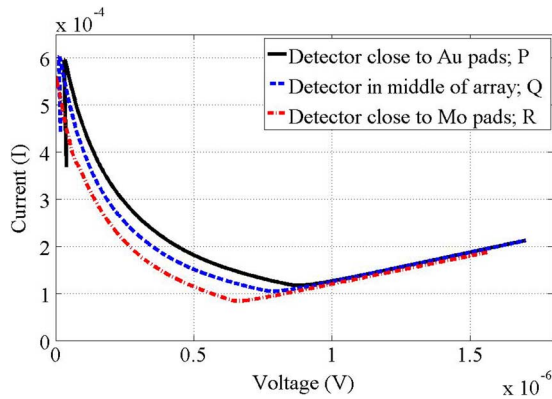
Fig. 5. IV curves of three detectors at different positions on the array chip. The detector locations are shown in Fig. 4(a). Detectors near the Au pads require more bias power to enter the transition, which is consistent with a lower local bath temperature. The IV curves of detectors L, M, and N show a similar ordering.

order to understand the heat flow within the chip, we are developing a finite element analysis (FEA) using the commercially available package, COSMOSworks [14]. In the finite element model, thermal conductivities are computed using the formula $\kappa = (Cv\ell)/3$ where C is the volumetric heat capacity, v is the carrier velocity, and ℓ is the carrier mean free path. For Si, $\kappa_{si} = 0.48$ W/K.m $\times T^3$ and for 0.5 (0.1) um thick Au, $\kappa_{Au} = 22.3(4.5)$ W/K.m $\times T$.

The electron-phonon coupling in the Au is included by means of a thickness-dependent boundary layer resistance at the Au-Si interfaces, which can be obtained from $G = 5\xi V T^4 = 5\xi A.d_{AU}T^4$, where d_{AU} is the thickness of the Au film. The calculated impedance into the Au at the top (bottom) of the array is $z_{Au} = 24.41(5.18)$ K.m^2/W. We assume that the Au bonds keep the Au films on the top surface of the chip at the cryostat temperature of 80 mK. Further, we assume that each sensor is a 100 pW power source. The steady-state predictions of the FEA model are shown graphically in Fig. 4(a). It can be seen that the chip is coolest near the Au bonds on the bottom and right sides, and hottest far from the Au bonds on the top and left sides. Numerical predictions for the chip temperature are shown in Fig. 4(b). The FEA model predicts temperature variations as large as 20 mK across the chip.

Current-voltage (IV) curves from three detectors at different points on the chip are shown in Fig. 5. The ordering of the IV curves is consistent with the temperature distribution predicted by the model. More quantitative comparisons with the predictions of the FEA model are presently underway, along with measurements of the critical temperature of all the pixels since this parameter also has a strong affect on the IV curves.

The FEA model can also be used to assess strategies to mitigate on-chip heating. Predicted temperature profiles are shown in Fig. 4(b) for different increases in the Au thickness on the front and/or back sides of the chip. For reasonable thicknesses

(2 μm), the temperature gradient can be reduced by a factor of four. We are also working to add Au bonds to all sides of the chip, which should produce a further temperature reduction.

V. CONCLUSIONS AND FUTURE WORK

We have successfully used a microcalorimeter array to identify isotope-specific gamma-rays from a Pu sample. We fabricated an array with 66 detectors and 31 were used to acquire a high statistics Pu spectra. The resolution of the best 21 detectors was 120 eV FWHM, and the statistical error in the ^{240}Pu line intensity was found to be approximately 0.7%, comparable to the systematic error in a measurement with a germanium sensor. Further understanding of the detectors, multiplexer, and cryostat wiring can improve the detector resolution and the number of multiplexed detectors. For example, we performed finite element analysis of the detector array to understand its thermal properties. This analysis makes clear predictions for how to reduce on-chip heating. As a result, we anticipate populating a detector box with four improved arrays totaling 256 pixels in the coming months.

REFERENCES

[1] D. T. Chow, A. Loshak, M. L. van den Berg, M. Frank, T. W. Barbee, Jr., and S. E. Labov, in *Proc. SPIE*, 2000, vol. 4141, p. 67.

[2] B. L. Zink, J. N. Ullom, J. A. Beall, K. D. Irwin, W. B. Doriese, W. D. Duncan, L. Ferreira, G. C. Hilton, R. D. Horansky, C. D. Reintsema, and L. R. Vale, *Applied Physics Letters*, vol. 89, p. 124101, 2006.

[3] K. D. Irwin, *Physica C: Superconductivity*, vol. 368, p. 203, 2002.

[4] K. D. Irwin, M. D. Audley, J. A. Beall, J. Beyer, S. Delker, W. Doriese, W. Duncan, G. C. Hilton, W. Holland, C. D. Reintsema, J. N. Ullom, L. R. Vale, and Y. Xu, *Nuclear Instruments and Methods in Physics Research Section A: Accelerators, Spectrometers, Detectors and Assiciated Equipment*, vol. 520, p. 544, 2004.

[5] K. D. Irwin and G. C. Hilton, *Cryogenic Particle Detection*, C. Enss., Ed. Berlin, Germany: Springer-Verlag, 2005, vol. 99, pp. 63–149.

[6] J. N. Ullom, B. L. Zink, J. A. Beall, W. B. Doriese, W. D. Duncan, L. Ferreira, G. C. Hilton, K. D. Irwin, C. D. Reintsema, L. R. Vale, M. W. Rabin, A. Hoover, C. R. Rudy, M. K. Smith, D. M. Tournear, and D. T. Vo, in *IEEE Nuclear Science Symposium Conference Record*, 2005, vol. N29, p. 1.

[7] J. N. Ullom, M. F. Cunningham, T. Miyazaki, S. E. Labov, J. Clarke, T. M. Lanting, A. T. Lee, P. L. J. Yoon, and H. Spieler, *IEEE Trans. Applied Superconductivity*, vol. 13, p. 643, 2003.

[8] C. Rudy, D. Dry, A. Hoover, S. Lamont, D. Vo, M. Rabin, R. Horansky, J. Ullom, K. Irwin, W. Doriese, J. Beall, G. C. Hilton, B. Zink, and K. Chesson, in *Proceedings of the European Safeguards Research and Development Association 2007 Symposium*, Aix-en-Provence, France, May 22–24, 2007.

[9] C. D. Reintsema, J. A. Beall, S. Deiker, W. B. Doriese, G. C. Hilton, K. D. Irwin, S. W. Nam, L. R. Vale, J. N. Ullom, Y. Xu, J. Beyer, and M. E. Huber, *Review of Scientific Instrument*, vol. 74, p. 4500, 2003.

[10] W. B. Doriese, J. A. Beall, W. D. Duncan, L. Ferreira, G. C. Hilton, K. D. Irwin, C. D. Reintsema, J. N. Ullom, L. R. Vale, and Y. Xu, *Nuclear Instruments and Methods in Physics Research A*, vol. 559, p. 808, 2006.

[11] W. B. Doriese, J. A. Beall, S. Deiker, W. D. Duncan, L. Ferreira, G. C. Hilton, K. D. Irwin, C. D. Reintsema, J. N. Ullom, L. R. Vale, and Y. Xu, *Applied Physics Letters*, vol. 85, p. 4762, 2004.

[12] US Congress, Office of Technology Assessment, Nuclear Proliferation and Safeguards Praeger. Santa Barbara, CA, 1977.

[13] P. Karpius, D. Vo, M. Bacrania, J. Beall, W. Doriese, G. Hilton, A. Hoover, R. Horansky, K. Irwin, M. Rabin, C. Reintsema, C. Rudy, J. Ullom, and L. Vale *et al.*, *IEEE Trans. Nuclear Science*, 2008, submitted for publication.

[14] [Online]. Available: http://www.solidworks.com/Pages/products/cosmos/cosmosworks.html